Journal of Chemistry and Technologies, 2024, *32*(4), 908-915

Journal of Chemistry and Technologies

pISSN 2663-2934 (Print), ISSN 2663-2942 (Online).

journal homepage: http://chemistry.dnu.dp.ua
editorial e-mail: chem.dnu@gmail.com

UDC 548.5 + 546.74+631.833+544.174

CRYSTAL GROWTH AND OPTICAL PROPERTIES ANIZOTROPY OF α-$NiSO_4 \times 6H_2O$

Mykhailo J. Filep*[1,2], Krisztina A. Molnar[1], Marjan Yu. Sabov[1,2], Artem I. Pogodin[2], Mykhailo M. Pop[2], Zoltan Z. Csoma[1]

[1]*Ferenc Rákóczi II Transcarpathian Hungarian Institute, 6 Kossuth Sq., Beregovo, 90200, Ukraine*
[2]*Uzhhorod National University, 46 Pidgirna Str., Uzhhorod, 88000, Ukraine*
Received 26 November 2024; accepted 14 December 2024; available online 25 January 2025

Abstract

α-$NiSO_4 \times 6H_2O$ single crystal was grown by slow evaporation technique and characterized by X-ray powder diffraction, differential thermal analysis, UV-Vis–NIR, FTIR, and atomic absorption spectroscopy methods. Combination of differential thermal analysis, X-ray powder diffraction and atomic absorption spectroscopy indicates a purity and phase homogeneity of grown α-$NiSO_4 \times 6H_2O$ crystal. The crystal structures of α-$NiSO_4 \times 6H_2O$ was refinement by Rietveld method. The calculated lattice parameters are: *a* = 6.8000 Å, *c* = 18.3161 Å, Z=4, space group $P4_12_12$. Four plane-parallel plates with different orientation were prepared. The orientation of the obtained plane-parallel plates was determined by XRD and are as follows: (301), (001), (320) and (204). The optical characteristics – transmittance and optical energy gap of the crystal plates were determined. All the crystal plates are characterized by higher transmittance values in the UVB range than in the VIS and NIR. The transmittance of single crystal plates decreases in the order (204) > (301) > (320) > (001). The band gap E_g values were determined by Tauc equation. Obtained E_g are in the range of 6.43–6.47 eV.

Keywords: growth from solutions; optical transmission spectra; thermal analysis; band gap; X-ray diffraction.

РІСТ КРИСТАЛІВ ТА АНІЗОТРОПІЯ ОПТИЧНИХ ВЛАСТИВОСТЕЙ α-$NiSO_4 \times 6H_2O$

Михайло Й. Філеп[1,2], Крістіна А. Молнар[2], Мар'ян Ю. Сабов[1,2], Артем І. Погодін[2], Михайло М. Поп[2], Золтан З. Чома[1]

[1]*Закарпатський угорський інститут ім. Ф. Ракоці II, пл. Кошута, 6, м. Берегово, 90202*
[2]*ДВНЗ «Ужгородський національний університет», вул. Підгірна 46, м. Ужгород, 88000*

Анотація

Монокристали α-$NiSO_4 \times 6H_2O$ було вирощено методом повільного випаровування з водного розчину та охарактеризовано методами порошкової рентгенівської дифракції, диференціального термічного аналізу, оптичної спектроскопії у широкому діарпазоані та атомно-абсорбційної спектроскопії. Комбінація результатів диференціального термічного аналізу, порошкової рентгенівської дифракції та атомно-абсорбційної спектроскопії вказує на фазову гомогенність вирощених монокристалів α-$NiSO_4 \times 6H_2O$. Кристалічну структуру α-$NiSO_4 \times 6H_2O$ було уточнено методом Рітвельда. Розраховані параметри ґратки становлять: *a* = 6.8000 Å, *c* = 18.3161 Å, Z=4, просторова група $P4_12_12$. Було підготовлено чотири плоскопаралельні пластини різної орієнтації. Орієнтацію отриманих плоскопаралельних пластин було визначено методом РФА, і вони відносяться до наступних площин: (301), (001), (320) та (204). Було визначено оптичні характеристики – пропускання та оптична ширина забороненої зони кристалічних пластин. Усі кристалічні пластини характеризуються вищими значеннями пропускання в УФ-діапазоні, ніж у видимому та ближньому ІЧ. Пропускання монокристалічних пластин зменшується в ряду (204) > (301) > (320) > (001). Значення ширини забороненої зони E_g були визначені за рівнянням Тауца. Отримані значення E_g знаходяться в діапазоні 6.43–6.47 еВ.

Ключові слова: вирощування з розчинів; спектри оптичного пропускання; термічний аналіз; ширина забороненої зони; рентгенівська дифракція.

**Corresponding author: e-mail: mfilep23@gmail.com*

doi: 10.15421/jchemtech.v32i4.316209

Journal of Chemistry and Technologies, 2024, *32*(4), 908-915

Inrtoduction

Nickel sulfate forms a significant number of hydrates $NiSO_4 \times nH_2O$ (n = 1-9) [1; 2]. However, the most actively studied is a hexahydrate $NiSO_4 \times 6H_2O$, also known as retgersite [3]. $NiSO_4 \times 6H_2O$ (NSH) is a well-known material which attracts considerable attention due to their wide range of properties: piezoelastic [4], magnetic [5], catalityc [6–10], electrochemical [11] and other [12–14] However, the main field of application of $NiSO_4 \times 6H_2O$ is a selective UV filter and UV detector [15–18], which is confirmed by the available commercial offers [19; 20] This is due to a high transmittance in the narrow spectral range of 200–300 nm, which makes them promising working elements in "solar-blind" technology [21; 22]. The optical properties of these crystals have been studied on samples oriented in the (001) plane [23; 24] or are not specified.

$NiSO_4 \times 6H_2O$ exist in two polymorph forms, namely α-$NiSO_4 \times 6H_2O$ (deep emerald-green) and β-$NiSO_4 \times 6H_2O$ (bluish green) [25]. α-NSH is a low temperature modification, which are formed by spontaneous nucleation from aqueous solution at temperatures below 55°C [26]. α-NSH crystallize in tetragonal crystal system, space group (SG) $P4_12_12$ and the unit cell parameters *a* = 6.790 Å, *c* = 18.305 Å and Z = 4 [27]. The β-NSH (mineral nickelhexahydrite) belong to monoclinic system, SG C2/c with parameters *a* =9.880 Å, *b* = 7.228 Å, *c* = 24.1300 Å, β =98.38° and Z = 8 [28].

Mainly, the study of the optical properties of α-$NiSO_4 \times 6H_2O$ crystals is carried out on samples oriented in the plane (001). This is due to a good cleavage on {001} along planes. At the same time, there is no information on the optical properties of α-NSH crystals oriented relative to different crystallographic planes. The aim of this work is to investigate the anisotropy of the optical properties of oriented α-$NiSO_4 \times 6H_2O$ crystal samples.

Experimental

Crystal growth and plates preparation

Single crystals of α-$NiSO_4 \times 6H_2O$ were grown from aqueous solution by the slow evaporation method. The starting solution was prepared using crystalline $NiSO_4 \times 6H_2O$ of high purity and bidistilled water. The concentration of the $NiSO_4$ solution was 0.15 mol/dm^3, and the pH of the solution was adjusted to 2 with 4 mol/dm^3 H_2SO_4 (controlled by a WTW inoLab Multi 9620 IDS). The $NiSO_4$ solution was kept in a LabExpert 1021 thermostat at 42 °C until the crystal seed appeared, and further single-crystal growth was carried out at 25 °C. The total growth time was 30 days. As a result, optically transparent and homogeneous emerald-green crystals with a typical habitus were obtained (Fig. 1).

The Ni^{2+} content in single crystals was determined using an Agilent 240AA atomic absorption spectrophotometer. The analysis was performed in the flame of an acetylene-air mixture at a wavelength of 429 nm. It was found that the Ni^{2+} content in the sample under study (m = 0.267 g), C_{Exp} = 587.0 mg/dm^3, is close to the theoretically calculated C_{calc} = 596.5 mg/dm^3.

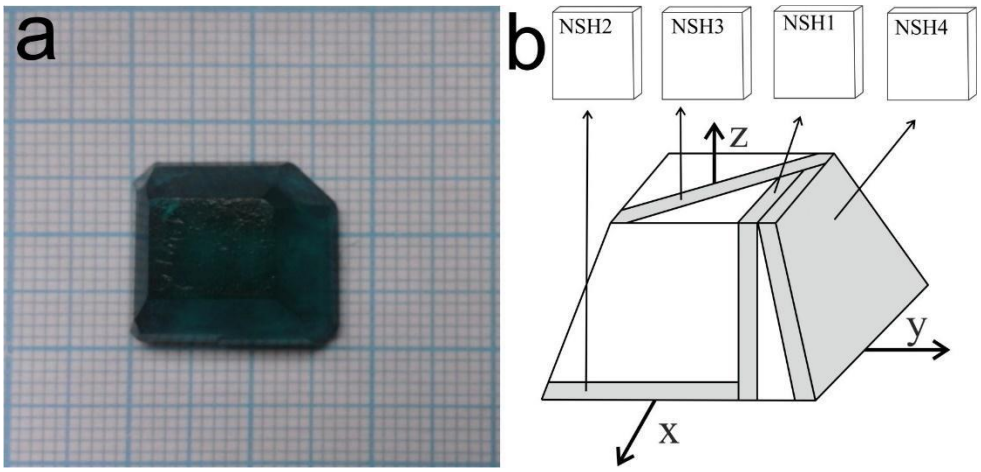

Figure 1. General view of α-$NiSO_4 \times 6H_2O$ single crystal (a) and scheme of single crystal plate selection (b)

Four plane-parallel plates marked as NSH1, NSH2, NSH3 and NSH4 with different crystallographic orientations were cut from the grown α-$NiSO_4 \times 6H_2O$ single crystal. The surface of the plates was prepared for further measurements according to the method [29].

Investigation methods

The thermal analysis was carried out in the temperature range of 20–600 °C in atmospheric

Journal of Chemistry and Technologies, 2024, *32*(4), 908-915

air using quartz containers with a heating rate of 12 °C/min. Pre-annealed Al_2O_3 was used as a reference material. The temperature detector is a combined chromel/alumel thermocouple (type K).

The phase analysis of the crystals was studied using an AXRD Benchtop diffractometer equipped with a DECTRIS MYTHEN2 R 1D hybrid detector using Ni filtered CuK_α radiation in the Bragg-Brentano θ/2θ mode. The scans were performed in the angle range of 10–120° 2θ with a dynamic region of interest and an exposure time of 1 s. The phase analysis was performed using the PDAnalysis (supplied by Proto Manufacturing) program. The lattice parameters were calculated using the EXPO 2014 [30] by Rietveld refinement method [31; 32]. The crystal structure was visualized using VESTA 3.5.4 [33].

The optical parameters of the crystals were studied using inSpect UV-1700 (spectral range 190–1100 nm) and Shimadzu IR Tracer-100 (spectral range 1265–14000 nm) spectrophotometers in transmission mode For microstructural studies, a METAM-R1 metallographic microscope was used.

Results and discussion

Characterization of bulk α-$NiSO_4$×$6H_2O$ single crystal

The grown α-$NiSO_4$×$6H_2O$ single crystal is phase homogeneous, which is confirmed by XRD studies. The experimental and calculated powder patterns (Fig.2) are in good agreement, which is confirmed by the shape of the difference curve. The crystal structures of α-$NiSO_4$×$6H_2O$, reported in Ref. [27], was used as structural models for the analysis by the Rietveld refinement method. The calculated parameters of the α-$NiSO_4$×$6H_2O$ cell are as follows: *a*= 6.8000 Å, *c*= 18.3161 Å, Z=4 (Fig. 2).

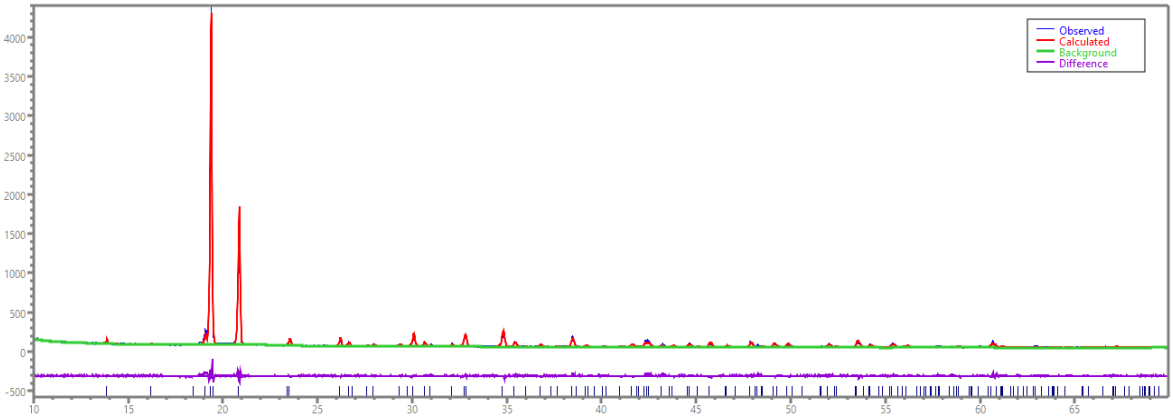

Fig. 2. Experimental (blue line), calculated (red line) and difference (purple) powder patterns of the grown α-$NiSO_4$×$6H_2O$

The structure of α-$NiSO_4$×$6H_2O$ is formed by two types of polyhedra: $[SO_4]$ tetrahedra and $[Ni(H_2O)_6]$ octahedra. All polyhedra $[Ni(H_2O)_6]$ and $[SO_4]$ are isolated from each other, since they do not have any common atoms, but are connected to each other only by hydrogen bonds (Fig. 3). The $[Ni(H_2O)_6]$ and $[SO_4]$ polyhedra are located at the same height within the cell (parallel to the xy plane) and are surrounded by 4 polyhedra of another type. These planes are equidistant from each other (d ~4.57 Å). This structure results in good cleavage perpendicular to the z-axis.

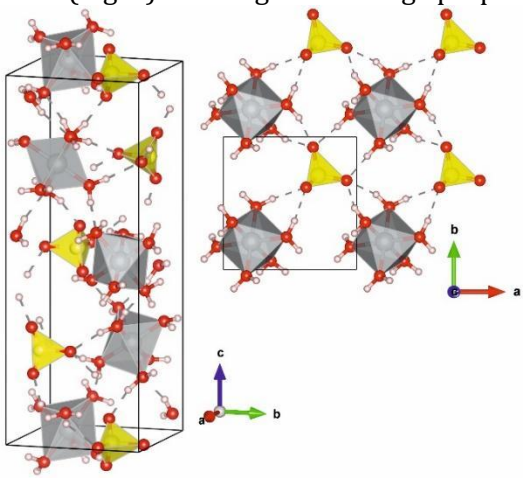

Fig.3. Unit cell of α-$NiSO_4$×$6H_2O$

Journal of Chemistry and Technologies, 2024, *32*(4), 908-915

The heating curve of α-$NiSO_4$×$6H_2O$ is characterized by the presence of three endothermic effects at 105, 126, and 394 °C. The effect at 105°C is of low intensity and most likely corresponds to the evaporation of water adsorbed on the crystal surface. The effects at 126 °C and 394°C are accompanied by a significant thermal effect and correspond to a stepwise dehydration process of α-$NiSO_4$×$6H_2O$ with the formation of anhydrous yellow $NiSO_4$, which was confirmed by XRD. The recorded final mass change Δm = 46.0 % is in good agreement with the theoretical one (Δm = 41 %).

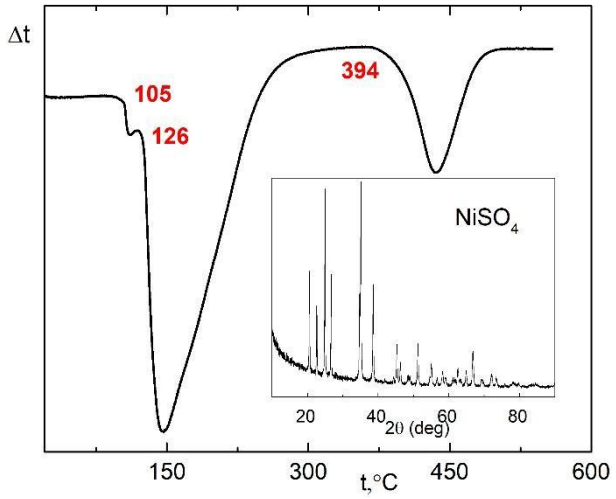

Fig. 4. Heating curve of α-$NiSO_4$×$6H_2O$. The inset shows the powder pattern of anhydrous $NiSO_4$

Properties of single crystal plates of α-$NiSO_4$×$6H_2O$

The orientation of the obtained plane-parallel plates was determined by XRD (Fig. 5). For all samples, the presence of a diffraction peak corresponding to one of the crystallographic planes is observed: sample NSH1 is oriented along the (301) plane, sample NSH2 – along the (001) plane, sample NSH3 is oriented along the (320) plane, and sample NSH4 is oriented along the (204) plane.

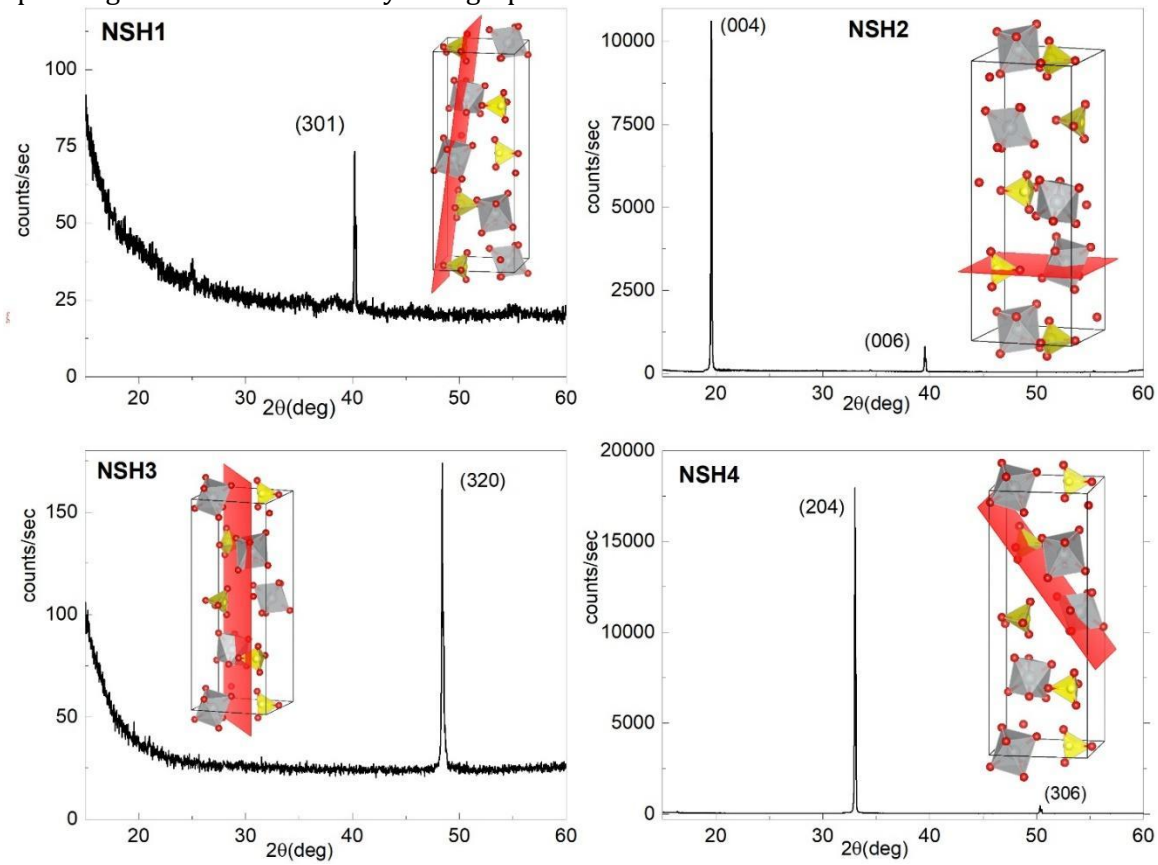

Fig. 5. XRD patterns of the prepared single crystal plates of α-$NiSO_4$×$6H_2O$

Journal of Chemistry and Technologies, 2024, *32*(4), 908-915

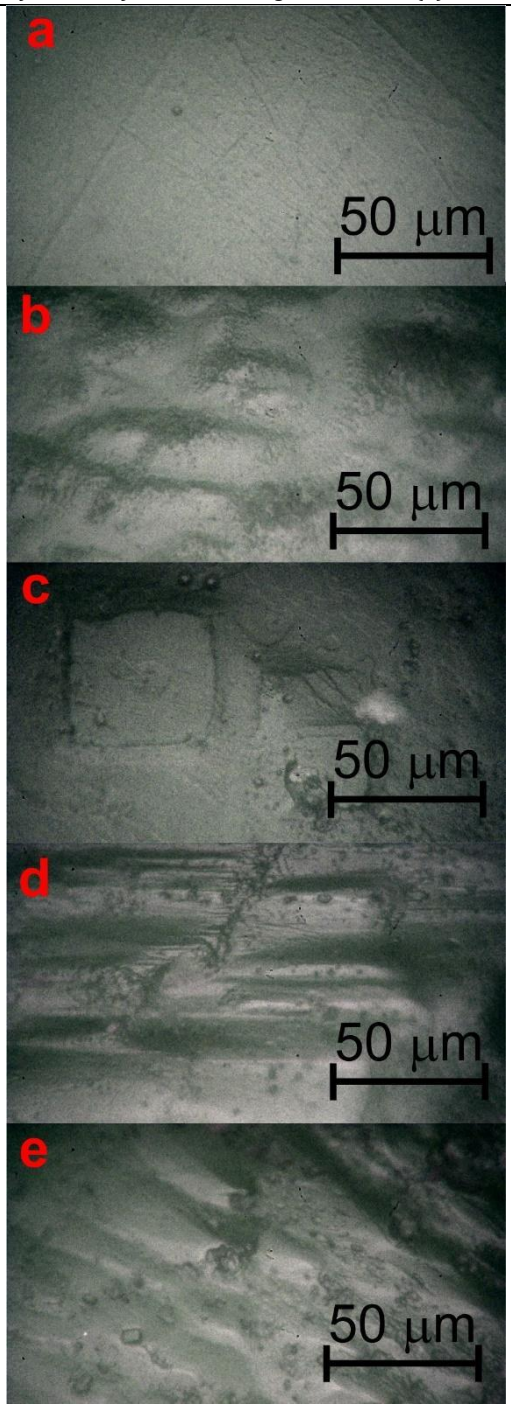

Fig. 6. Surface of untreated plate NSH2 (a) and etched plates NSH1 (b), NSH2 (c), NSH3 (d), NSH4 (e)

To study the optical transmission spectra of α-$NiSO_4 \times 6H_2O$ crystals in the UV-VIS and IR ranges, plane-parallel samples with a thickness of 0.030–0.079 cm were made. The transmittance spectra (UV-VIS-NIR range) of the oriented α-$NiSO_4 \times 6H_2O$ plates (Fig. 7a), in the studied range, contain absorption bands that are typical [29; 33] for the complex cation $[Ni(H_2O)_6]^{2+}$ (d^8 configuration) and correspond to optical transitions: $^3A_{2g} \rightarrow {}^3T_{1g}(P)$ (~385 nm), $^3A_{2g} \rightarrow {}^3T_{1g}(F)$ (~645 nm), $^3A_{2g} \rightarrow {}^1E_g$ (~710 nm) and $^3A_{2g} \rightarrow {}^3T_{2g}$ (~1100 nm).

All the crystal plates are characterized by higher transmittance values in the UVB range than in the VIS and NIR, and the maximum transmittance is observed for plates NSH1 and NSH4. The FTIR spectra of the studied α-$NiSO_4 \times 6H_2O$ plates are characterized by the presence of two regions – 1265–2500 nm, characterized by the presence of transmission bands (up to ~40 %) and a region of strong absorption (>2500 nm), which is most likely due to the presence of the Ni^{2+} ion (Fig.7.b).

Journal of Chemistry and Technologies, 2024, *32*(4), 908-915

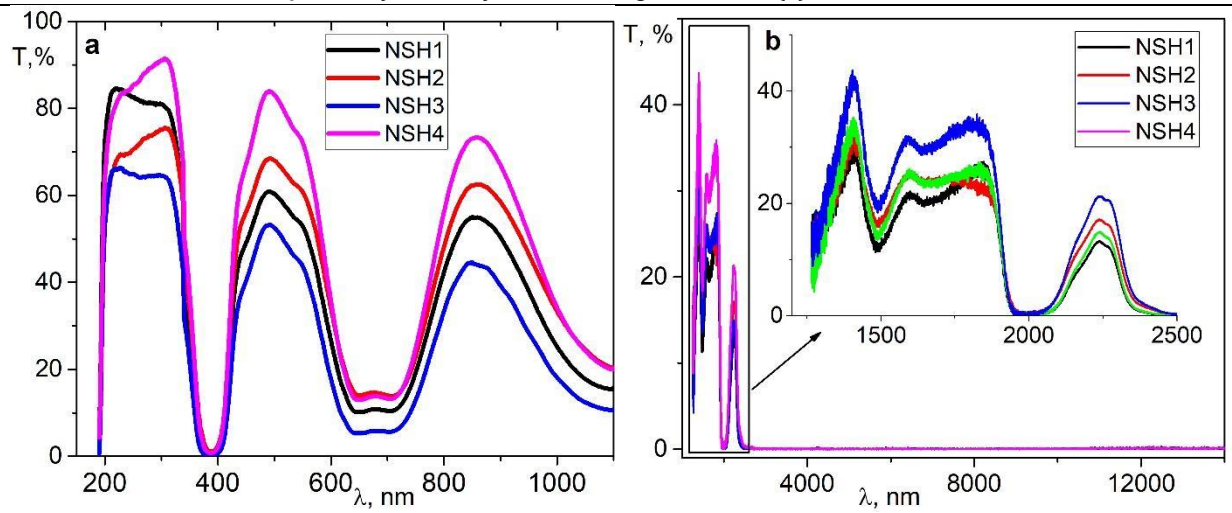

Fig. 7. Transmittance spectra of α-$NiSO_4$×6H_2O plates in the UV-VIS-NIS (a) and IR (b) ranges

Table 1

Thickness and optical characteristics of α-$NiSO_4$×6H_2O plates

Sample	Orietation (hkl)	Thickness d, cm	T_{max}, %(at 270 nm)	lnα (at 270 nm)	E_g, eV
NSH1	(301)	0.058	81	1.27	6.44
NSH2	(001)	0.030	73	2.34	6.45
NSH3	(320)	0.079	64	1.72	6.47
NSH4	(204)	0.063	88	0.71	6.43

Since the thickness of the plates is not the same, the absorption coefficient α (for the UV-VIS-NIS range) was calculated. The absorption coefficient α takes into account the thickness of the sample, which allows us to estimate the throughput of samples with different thicknesses. The absorption coefficient α was calculated using the formula [34,35]:

$$\alpha = -\ln(1/T) / d \quad (1)$$

where d – is the thickness of a plate and T – is transmittance.

The analysis of the spectral dependences of lnα indicates that the highest transmittance is characterized by sample NSH4, and the lowest is characterized by sample NSH2. The transmittance of single crystal plates decreases in the order NSH4 > NSH1 > NSH3 >NSH2. This trend is also clearly visible when comparing the maximum transmittance T and thickness d (Table 1). Thus, the sample NSH2, having the smallest thickness (~ 1/2 d relative to the others), does not exhibit the highest transmittance.

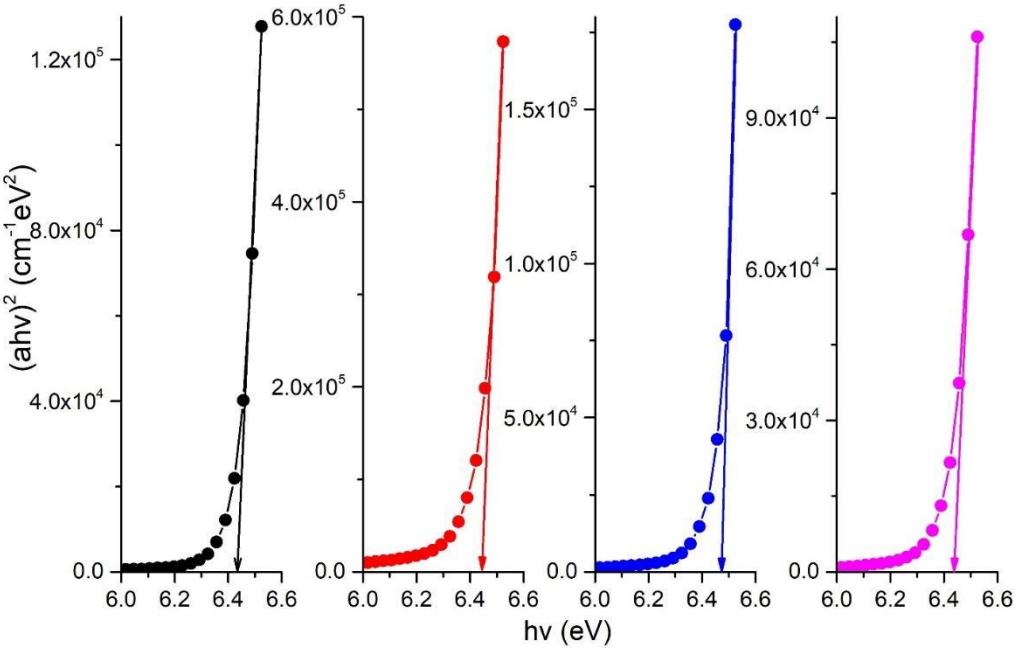

Fig. 8. Tauc's plot for plane-parallel plates of α-$NiSO_4$×6H_2O

The band gap E_g was determined for the studied α-$NiSO_4$×$6H_2O$ samples. For this purpose, the Tauc equation [35,36] was used, which combines the absorption coefficient (α) and the frequency of light (ν) with the band gap energy (E_g), and B is the edge width parameter. The parameter m was set as 1/2, which corresponds to a direct allowed transition.

$$\alpha h\nu = B(\alpha h\nu - E_g)^m \quad (2)$$

To determine the band gap E_g value, the corresponding dependencies $(\alpha h\nu)^2$ vs hν were constructed, and the corresponding values of E_g were determined by extrapolating the linear section to the intersection of the x-axis. The values of E_g are close (within the determination error) and are in the range of 6.43–6.47 eV.

Conclusions

α-$NiSO_4$×$6H_2O$ crystal was successfully grown by slow evaporation technique. Grown crystal was characterized by different methods. XRD results combined with atomic absorption spectroscopy analysis indicate a phase homogeneity of obtained crystals. The optical parameters in the UV-VIS-NIR and IR ranges were studied on plane-parallel α-$NiSO_4$×$6H_2O$ plates of different orientations. It was found that the samples with orientation (102) have the highest transmittance.

Acknowlegements

The work was supported by the Visegrad+ project #22330251.

References

[1] Maneva, M., Rizova, D., Genov, L., Liptay, G. (1999). On the thermal decomposition of $NiSO_4$·nH_2O (n=7,6,4,1) and of their deuterated analogs. *Journal of Thermal Analysis*. 36, 915–922. https://doi.org/10.1007/BF01904627

[2] Fortes, A.D., Knight, K.S., Gibbs, A.S., Wood, I.G. (2018). Crystal structures of $NiSO_4$·$9H_2O$ and $NiSO_4$·$8H_2O$: magnetic properties, stability with respect to morenosite ($NiSO_4$·$7H_2O$), the solid-solution series $(Mg_xNi_{1-x})SO_4$·$9H_2O$. *Phys Chem Minerals*. 45, 695–712. https://doi.org/10.1007/s00269-018-0956-z

[3] Sejkora, J., Škácha, P., Vrtiška, L., Dolníček, Z., Jindra, J. (2023). Retgersite from mine dump of the Lill shaft, Březové Hory ore district, Příbram (Czech Republic). *Bulletin Mineralogie Petrologie. 31*(1), 89–94. https://doi.org/10.46861/bmp.31.089

[4] Arbeck, D., Haussühl, E., Bayarjagal, L., Winkler, B., Paulsen, N., Haussühl, S., Milman, V. (2010). Piezoelastic properties of retgersite determined by ultrasonic measurements. *Eur. Phys. J.* B73, 167–175. https://doi.org/10.1140/epjb/e2009-00423-9

[5] Aswathappa, S., Dai, L., Sathiyadhas, S.J.D., Amalapushpam, M.B.D.S., Thangavel, V., Vijayakumar, V.N., Kumar, R.S., Almansour, A.I. (2024). Unveiling the correlation between the structure and property of the amorphous state of hydrated nickel sulfate (NiSO4·6H2O) induced by acoustic shock waves – An X-ray diffraction, thermal calorimetric and dielectric spectroscopic approach. *Materials Science and Engineering: B. 302*, 117205. https://doi.org/10.1016/j.mseb.2024.117205.

[6] Matsumoto, A., Ozawa, H., Inumarua, A., Soai, K. (2015). Asymmetric induction by retgersite, nickel sulfate hexahydrate, in conjunction with asymmetric autocatalysis. *New J. Chem*. 39. 6742–6745. https://doi.org/10.1039/C5NJ01459J .

[7] Guezane Lakoud, S., Merabet-Khelassi, M., Aribi-Zouioueche, L. (2016). $NiSO_4$·$6H_2O$ as a new, efficient, and reusable catalyst for the α-aminophosphonates synthesis under mild and eco-friendly conditions. *Res Chem Intermed*. 42, 4403–4415. https://doi.org/10.1007/s11164-015-2283-z.

[8] Li, L., Chavan S., Ganjkhanlou Y., Groppo E., Sagstuen E., Bordiga S., Olsbye U., Jens K.-J. (2022). Characterization of the $NiSO_4$ site on a $NiSO_4$-ReO_x/γ-Al_2O_3 catalyst for tandem conversion of ethylene to propylene. *Applied Catalysis A: General*. 637, 118598. https://doi.org/10.1016/j.apcata.2022.118598.

[9] Ling Y., Chen X., Tong H., Guan W., Chen P., Huang Z., Liang C. (2021). Modulating the Interaction of $NiSO_4$ and Nb_2O_5 Boosts the Dimerization of Propylene. *Industrial & Engineering Chemistry Research*. 60 (19), 6959-6970. https://doi.org/10.1021/acs.iecr.1c00142.

[10] Shoair A.G.F., Almalki A.S.A., Shanab M.M.A.H., Sheta A.M., El-Basiony A., El-Ghamaz N.A., Nasef H.A., Khalaf H.A. (2023) Unlocking the Potential of $NiSO_4$·$6H_2O$/NaOCl/NaOH Catalytic System: Insights into Nickel Peroxide as an Intermediate for Benzonitrile Synthesis in Water. *J. Nanotechnol.* 2023, 9940845. https://doi.org/10.1155/2023/9940845 .

[11] Pan Y., Chen D., Fan Y., Zuo J., Yang Q., Qiu F., Qiu L., Song H., Zhang S. (2023). Highly-sensitive and anti-interferential electrochemical determination of hazardous metronidazole using w-$NiSO_4$·NiS_2 coated ZIF-67-derived cobalt/nitrogen-doped carbon. *Colloids Surf., A.* 666, 131293. https://doi.org/10.1016/j.colsurfa.2023.131293.

[12] Ali A.-R., Lackner J., Cerdas F., Herrmann C. (2023). Analysis of nickel sulphate datasets used in lithium-ion batteries. Procedia CIRP. 116, 348-353. https://doi.org/10.1016/j.procir.2023.02.059.

[13] Ma, Y., Svärd, M., Xiao X., Sahadevan, S.A., Gardner, J., Olsson, R.T., Forsberg, K. (2022). Eutectic freeze crystallization for recovery of $NiSO_4$ and $CoSO_4$ hydrates from sulfate solutions. *Sep. Purif. Technol*. 286, 120308. https://doi.org/10.1016/j.seppur.2021.120308.

[14] Li W., Qu J.-e., Cao Z., Wang, H. (2020) Effects of $NiSO_4$ Concentration on the Coloring Performance and Corrosion Resistance of the Colored Film on 304 Stainless Steel. *Coatings*. 10, 598. https://doi.org/10.3390/coatings10060598

[15] Thirupathy J. (2021). An Investigation of the Thermal and Dielectric Properties of Nickel Sulfate Hexahydrate Single Crystal for Sensors, Bandpass Filters and Optical Applications. *J. Electron. Mater*. 50, 3385–3391. https://doi.org/10.1007/s11664-021-08830-x .

[16] Kathiravan, P., Balakrishnan, T., Srinath, C., Ramamurthi, K., Thamotharan S. (2016). Growth and characterization of α-nickel sulphate hexahydrate single crystal. Karbala International *Journal of Modern Science*. 2, 226–238. https://doi.org/10.1016/j.kijoms.2016.08.002 .

[17] Masilamani, V., Shanthi, J., Sheelarani, V. (2014). Growth and Analysis of NSH and KMNSH Crystals by Slow Evaporation Technique. *International Scholarly Research Notices.* 678567. https://doi.org/10.1155/2014/678567.

[18] George R., Patel I.B., Rathod K.T. (2021) Growth and photoluminescence study of nickel sulfate doped Zinc tris-Thiourea Sulfate (ZTS) crystal. Mater. Today: Proc. 37 (2), 2189–2192. https://doi.org/10.1016/j.matpr.2020.07.649 .

[19] Eksmaoptics, Optical Filters https://eksmaoptics.com/optical-components/optical-filters/

[20] Key Photonics, Optical Filters https://www.key-photonics.co.uk/optical-filters.php

[21] Oliveira Neto J.G. de, Marques J.V., Silva Filho J.G. da, Antonelli E., Ayala A.P., Santos A.O. dos, Lang R. (2024) Mixed $(NH_4)_2Mn_{0.47}Cu_{0.53}(SO_4)_2(H_2O)_6$ Tutton salt: A novel optical material for solar-blind technology. *Optical Materials.* 157(3), 116400. https://doi.org/10.1016/j.optmat.2024.116400.

[22] Kalra A., Muazzam U.U.l., Muralidharan R., Raghavan S., Nath D.N. (2022). The road ahead for ultrawide bandgap solar-blind UV photodetectors. *J. Appl. Phys. 131*(15), 150901. https://doi.org/10.1063/5.0082348

[23] Hemmati, M., Rezagholipour, D. H. (2012). Unidirectional growth of α-$NiSO_4{\cdot}6H_2O$ crystal by Sankaranarayanan–Ramasamy (SR) method. *Crystal Research and Technology.* 47, 703–706. https://doi.org/10.1002/crat.201200011.

[24] Su G., He Y., Li Z., Jiang R., Zhu C., Yang S. (2000). Directional solution growth of cylindrical α-$NiSO_4{\cdot}6H_2O$ crystal. *Journal of Crystal Growth*. 213, 99-102. https://doi.org/10.1016/S0022-0248(00)00304-3.

[25] Anthony J.W., Bideaux R.A., Bladh K.W., Nichols M.C. (2003). *Handbook of mineralogy, Vol. V. Borates, Carbonates, Sulfates*. Mineral Data Publishing, Tucson, Arizona.

[26] Jenssen I.B., Bøckman O., Andreassen J.-P., Ucar S. (2021). The Effect of Reaction Conditions and Presence of Magnesium on the Crystallization of Nickel Sulfate. *Crystals*. 11, 1485. https://doi.org/10.3390/cryst11121485.

[27] Sivakumar A,. Sahaya Jude Dhas S., Thirupathy J., Reddy K.P.J., Kumar R.S., Almansour A.I., Chakraborty S., Martin Britto Dhas S.A. (2022). Switchable crystal–amorphous states of $NiSO_4{\cdot}6H_2O$ induced by a Reddy tube. *New Journal of Chemistry.* 46, 5091–5099. http://doi.org/10.1039/D2NJ00129B.

[28] Gerkin R.E., Reppart W.J. (1988). Structure of monoclinic nickel(II) sulfate hexahydrate. *Acta Crystallographica Section C*. 44, 1486-1488. https://doi.org/10.1107/S0108270188004238.

[29] Filep M., Molnár K., Sabov M., Csoma Z., Pogodin A. (2021). Structural, thermal, and optical properties of Co^{2+} and Mg^{2+} doped $K_2Ni(SO_4)_2{\bullet}6H_2O$ single crystals. *Optical Materials. 122,* Part A. 111753. https://doi.org/10.1016/j.optmat.2021.11175 3.

[30] Altomare A., Cuocci C., Giacovazzo C., Moliterni A., Rizzi R., Corriero N., Falcicchio A. (2013). A kit of tools for phasing crystal structures from powder data. *J. Appl. Crystallogr.* 46, 1231–1235. https://doi.org/10.1107/S0021889813013113

[31] Xiao J.; Song Y.; Li Y. (2023). Comparison of Quantitative X-ray Diffraction Mineral Analysis Methods. *Minerals*. 13, 566. https://doi.org/10.3390/min13040566.

[32] Runčevski T., Brown C.M. (2021) The Rietveld Refinement Method: Half of a Century Anniversary. *Cryst. Growth Des. 21*(9), 4821-4822. https://doi.org/10.1021/acs.cgd.1c00854 .

[33] Momma K., Izumi F. (2011). VESTA 3 for three-dimensional visualization of crystal, volumetric and morphology data. *J. Appl. Crystallogr*. 44, 1272–1276. https://doi.org/10.1107/S0021889811038970

[34] Triest M., Bussière G., Bélisle H., Reber C. (2000). Why does the middle band in the absorption spectrum of $Ni(H_2O)_6^{2+}$ have two maxima? *J. Chem. Educ*. 77, 670. https://doi.org/10.1021/ed077p670.2.

[35] Allaham M., Dallaev R., Burda D., Sobola D., Nebojsa A., Knápek A., Mousa M.S., Kolařík V. (2024). Energy gap measurements based on enhanced absorption coefficient calculation from transmittance and reflectance raw data. *Phys. Scr*. 99 (2), 025952. https://doi.org/10.1088/1402-4896/ad1cb8.

[36] Jubu, P.R., Danladi, E., Ndeze, U.I., Adedokun, O., Landi, S., Haider, A.J., Adepoju, A.T., Yusof, Y., Obaseki, O.S., Yam F.K. (2024) Comment about the use of unconventional Tauc plots for bandgap energy determination of semiconductors using UV–Vis spectroscopy. *Results in Optics*. 14, 100606. https://doi.org/10.1016/j.rio.2024.100606.

[37] Haryński, Ł., Olejnik, A., Grochowska, K., Siuzdak, K. (2022). A facile method for Tauc exponent and corresponding electronic transitions determination in semiconductors directly from UV–Vis spectroscopy data. *Optical Materials*. 127, 112205. https://doi.org/10.1016/j.optmat.2022.112205.